Surface modes and breathers in finite arrays of nonlinear waveguides

Yu. V. Bludov[1] and V. V. Konotop[1,2]
[1]*Centro de Física Teórica e Computacional, Universidade de Lisboa, Complexo Interdisciplinar, Avenida Professor Gama Pinto 2, Lisboa 1649-003, Portugal*
[2]*Departamento de Física, Faculdade de Ciências, Universidade de Lisboa, Campo Grande, Ed. C8, Piso 6, Lisboa 1749-016, Portugal*
(Received 9 April 2007; revised manuscript received 5 July 2007; published 8 October 2007)

We present the complete set of symmetric and antisymmetric (*edge* and *corner*) surface modes in finite one- and two-dimensional arrays of waveguides. We provide classification of the modes based on the anticontinuum limit, study their stability and bifurcations, and discuss relation between surface and bulk modes. We put forward existence of *surface breathers*, which represent two-frequency modes localized about the array edges.

DOI: 10.1103/PhysRevE.76.046604 PACS number(s): 42.65.Tg, 42.65.Sf, 42.65.Wi

I. INTRODUCTION

Waves at surfaces and interfaces are known to exhibit peculiar properties. Localized electronic states at a crystal edge, discovered by Tamm [1], were the first example of such phenomena. Later on it was found that surfaces and interfaces are able to sustain localized waves which attracted a great deal of attention in different areas of physics, particularly due to the variety of practical applications, like plasmonic waveguides [2], sensors [3], etc. Recently it was predicted theoretically [4] and observed experimentally [5], that at the edge of a semi-infinite one-dimensional (1D) array of nonlinear waveguides there can exist discrete surface solitons. Modes localized at finite distances from the edge were considered in [6] and surface gap solitons between uniform media and periodic lattice were reported in [7]. Different types of surface modes in two dimensional (2D) arrays were studied in [8,9].

Structures with two surfaces give rise to different properties of surface modes. For example, interaction of the two surface polaritons, supported by each surface of a metallic film, results in creation of symmetric and antisymmetric modes [10], which in turn originate polariton-assisted extraordinary transmittancy of the film [11].

In this paper we describe discrete (*edge* and *corner*) surface modes in finite 1D and 2D arrays of nonlinear waveguides. We show that they can be classified on the basis of the anticontinuum (AC) limit, similarly to the classification of intrinsic localized modes introduced in [12], and in this way the *complete* families of modes can be identified. We show that surface modes can bifurcate either with other surface or with bulk modes and study the mode stability. We also report a different type of surface excitations—*surface breathers*—which represent two-periodic excitations localized in the vicinity of the array edges.

II. SURFACE AND BULK MODES

A. The model and terminology

We start with a finite array of M nonlinear waveguides described by the discrete nonlinear Schrödinger (DNLS) equation [13],

$$i\dot{q}_n + \sum_{n'=1}^{M} (\delta_{n',n+1} + \delta_{n',n-1}) q_{n'} + \sigma |q_n|^2 q_n = 0. \qquad (1)$$

Here $\dot{q}_n \equiv dq_n/d\zeta$, ζ is the propagation coordinate, q_n is the dimensionless field amplitude in the nth waveguide ($n=1,\ldots,M$), $\sigma=1$ and $\sigma=-1$ stand for focusing and defocusing nonlinearities. We concentrate on modes having definite parity imposing $q_n=q_{M+1-n}$ for symmetric and $q_n=-q_{M+1-n}$ for antisymmetric modes. Equation (1) possesses two integrals of motion: the Hamiltonian $H=-\Sigma_{n=1}^{M-1}(q_{n+1}^* q_n + q_{n+1} q_n^*) - \frac{\sigma}{2}\Sigma_{n=1}^{M}|q_n|^4$ and the total power $P=\Sigma_{n=1}^{M}|q_n|^2$.

It worthwhile to emphasize that the DNLS equation (1) is a widely used model in condensed matter physics [14] and in the theory of Bose-Einstein condensates loaded in optical lattices [15], which makes the results reported below relevant for a rather wide class of the phenomena of the nonlinear physics of periodic and discrete structures.

Like in the well studied infinite case [16], stationary modes of Eq. (1) are searched in the form $q_n(\zeta) = Q_n \exp(-i\lambda\zeta)$, where λ is the propagation constant, and the resulting equations are

$$\lambda Q_n + \sum_{n'=1}^{M} (\delta_{n',n+1} + \delta_{n',n-1}) Q_{n'} + \sigma Q_n^3 = 0. \qquad (2)$$

The solutions for $\sigma=\pm 1$ are connected by the following symmetry reduction [12]: if the Q_n is a solution of Eq. (1) for a definite λ and $\sigma=+1$, then $(-1)^n Q_n$ is a solution for $-\lambda$ and $\sigma=-1$.

In order to describe the whole diversity of solutions and to classify them [12], one has to consider the AC limit [17]. To this end we rewrite Eq. (1) in terms of the rescaled stationary amplitudes $v_n = Q_n/\sqrt{|\lambda|}$ as

$$\sigma|\lambda| v_n (v_n^2 + \sigma s) + \sum_{n'=1}^{M} (\delta_{n',n+1} + \delta_{n',n-1}) v_{n'} = 0, \qquad (3)$$

where $s=\mathrm{sign}(\lambda)$, and consider the limit $|\lambda|\to\infty$. In this limit v_n become independent and for the case $\sigma s=-1$ acquire one of the three values: $v_n=-1$, $v_n=0$, and $v_n=+1$ ($1\le n\le M$). Thus, in the AC limit there exists $N_s=(3^{[(M+1)/2]}-1)/2$ sym-

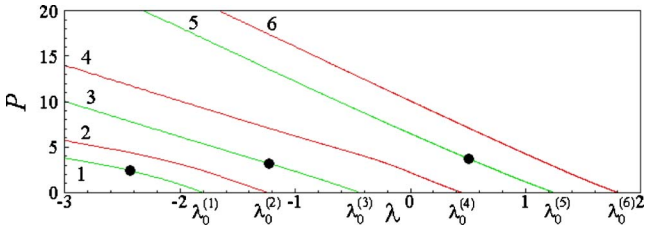

FIG. 1. (Color online) Dependence of power P vs the propagation constant λ for the bulk symmetric and antisymmetric modes in the case $\sigma=1$, $M=6$, which do not have the excitation threshold: 1—mode {00++00}, 2—mode {0+00−0}, 3—mode {+0−−0+}, 4—mode {+0−+0−}, 5—mode {+−++−+}, 6—mode {+−+−+−}. The bifurcation points with asymmetric modes are depicted by filled circles.

metric and $N_a=(3^{[M/2]}-1)/2$ antisymmetric modes (here square brackets signify the integer part), and each mode can be coded [12] by a sequence of M symbols −, 0, and +. The coding corresponds to the limit of the infinite power: i.e., in particular, "0" does not refer to the zero intensity of a waveguide at a finite input intensity (see Fig. 2, and discussion below). As an example, an array of three waveguides has four symmetric: {0+0}, {+++}, {+−+}, {+0+} modes, and one antisymmetric mode {+0−}. A sequence, consisting of symbols {+,0,−}, is termed a "word," a word having only zeros is referred to as "empty," and a word having no 0 (for example, {+−+}) is called a "simple" word. The number of symbols in a word is called the *length of the word*.

The first important property of the coding stems from the analytical continuation of the AC limit [17] to $|\lambda|>\lambda_{ac}$, where λ_{ac} is a constant (in the case of the infinite array $\lambda_{ac}\approx 5.4533$ [12]). This means that *all the words exhaust all possible modes of a finite array* existing for $\lambda>\lambda_{ac}$. Second, the AC limit allows one to introduce a definition for a *surface mode* as a code consisting of two simple words separated by an empty word, the latter having the length not less than the lengths of each of the simple words. For example, {+−+0000+−+} is a surface mode of an array of ten waveguides. All other modes will be referred to as *bulk modes*. The introduced terminology, being mathematically well defined, has relative physical meaning for finite λ: surface modes can bifurcate with bulk modes, both acquiring identical shapes in the bifurcation point.

B. Bulk modes

In the linear limit $P\to 0$ (or formally $\sigma\to 0$) Eq. (2) possesses M eigenvalues $\lambda_0^{(m)}=-2\cos[\pi m/(M+1)]$ corresponding to eigenmodes

$$Q_{0,n}^{(m)}=\sin\left(\frac{\pi nm}{M+1}\right),\quad m=1,\ldots,M. \tag{4}$$

Thus one can expect that M bulk modes have a linear limit and thus do not possess an intensity threshold of excitation: for these modes, when $\lambda\to\lambda_0^{(m)}$, the power $P^{(m)}$ of the mth mode ($m=1,\ldots,M$) approaches zero (see Fig. 1). In order to determine the dependence $P^{(m)}(\lambda)$ near the linear limit we follow the standard perturbation technique (see, e.g., [18]), and look for a solution of Eq. (2) in a form of the series

$$Q_n=\epsilon Q_{0,n}^{(m)}+\epsilon^3 Q_{2,n}^{(m)}+o(\epsilon^3), \tag{5}$$

$$\lambda=\lambda_0^{(m)}+\epsilon^2\lambda_2^{(m)}+o(\epsilon^2), \tag{6}$$

where we have introduced the small parameter $\epsilon=\sqrt{2P/(M+1)}\ll 1$. Substituting the above expansions into Eq. (2) and gathering the terms of the same order in ϵ, we rewrite Eq. (2) in the form of a set of equations:

$$\lambda_0^{(m)}Q_{j,n}^{(m)}+\sum_{n'=1}^{M}(\delta_{n',n+1}+\delta_{n',n-1})Q_{j,n'}^{(m)}=F_{j,n}^{(m)}. \tag{7}$$

Here $F_{0,n}^{(m)}=0$, $F_{2,n}^{(m)}=-\lambda_2^{(m)}Q_{0,n}^{(m)}-\sigma(Q_{0,n}^{(m)})^3$. As is clear, Eq. (7) for $j=0$ describes a linear eigenmode and therefore is automatically satisfied, while considering solvability conditions for $j=2$ (it is equivalent to orthogonality $F_{2,n}^{(m)}$ and $Q_{0,n}^{(m)}$), we obtain the corrections to the eigenvalues written in the form

$$\lambda=\lambda_0^{(m)}-\epsilon^2\sigma\frac{3+\delta_{m,(M+1)/2}}{4}. \tag{8}$$

It follows from Eq. (8) that each of M linear modes possesses its unique small-amplitude nonlinear analog (from all diversity of nonlinear modes only given M bulk modes have small-amplitude solution). This also proves that *no linear surface mode exists* (which corroborates the earlier findings for a semi-infinite array [6]). Moreover, from Eq. (8) it follows that in the small-amplitude limit these modes are characterized by the linear dependence of the mode total power upon the propagation constant:

$$P^{(m)}=\sigma(2M+2)\frac{\lambda_0^{(m)}-\lambda}{3+\delta_{m,(M+1)/2}}. \tag{9}$$

From Eq. (9) it is clear that powers of these modes are decaying for $\sigma=1$ and increasing for $\sigma=-1$ functions of λ. To single out the obtained modes in what follows they are referred to as *quasilinear* modes.

C. Bifurcations of quasilinear modes

When the power increases one of two scenarios of mode transformations is possible: either the branch of the quasilinear mode smoothly tends to a uniquely defined AC limit or at some λ_* (alternatively P_*) it bifurcates giving origin to some new solutions. As it is clear, each mode can bifurcate either with a mode of the same symmetry or with an asymmetric mode (which in principle does not possess any symmetry, but in the bifurcation point acquires the given symmetry). If the former even takes place then the quasilinear mode is naturally classified by its AC limit. While we leave analytical description of other cases for further studies, we mention that all numerical simulations we performed with a finite number of waveguides have shown that no bifurcations of the quasilinear modes with modes of the same symmetry occurs: only asymmetric modes bifurcate from the quasilinear ones. This allows us to use for the latter modes the classification deter-

mined by their symmetric AC limit (i.e., by a word describing symmetric ramification of the mode). Namely these notations are used in the figure captions and in the text whenever we speak about quasilinear modes.

To determine numerically the bifurcation points of the quasilinear modes we consider the continuation of the mode by the parameter λ (notice that contrary to the standard approach [12,17] now we "move" along the branch outward from the linear limit),

$$\frac{d\mathbf{Q}}{d\lambda} = -[D_Q\mathbf{F}]^{-1}\frac{\partial \mathbf{F}(\mathbf{Q},\lambda)}{\partial \lambda}, \tag{10}$$

where $\mathbf{Q}=\mathrm{col}(Q_n)$,

$$\mathbf{F}(\mathbf{Q},\lambda) = \mathrm{col}\left(\lambda Q_n + \sum_{n'=1}^{M}(\delta_{n',n+1}+\delta_{n',n-1})Q_{n'} + \sigma Q_n^3\right),$$

and the entries of the three-diagonal matrix $D_Q\mathbf{F}$ are

$$(D_Q\mathbf{F})_{n,n'} = \delta_{n,n'}(\lambda + 3\sigma Q_n^2) + \delta_{n,n'-1} + \delta_{n,n'+1}. \tag{11}$$

This continuation of the quasilinear modes is possible, while the matrix $D_Q\mathbf{F}$ is invertible, i.e., its determinant is not equal to zero. Thus the bifurcation point is determined by the equation $D \equiv D(\lambda) \equiv \mathrm{Det}|D_Q\mathbf{F}|=0$.

As we already mentioned, M quasilinear modes can bifurcate with asymmetric modes which is illustrated in Fig. 1 obtained for $M=6$. There all symmetric modes possess additional bifurcation points, denoted by filled circles. Although the consideration of modes without symmetry is beyond the scope of this paper, we now analyze analytically the simplest case of $M=2$ and $\sigma=1$ allowing the trivial solution. In that case there exists one antisymmetric mode $Q_{1,2}^2=1-\lambda$ (with code {+−}) and one symmetric mode $Q_{1,2}^2=-1-\lambda$ (with code {++}). Substituting the expressions for the field distribution of the antisymmetric mode {+−} into Eq. (11), we obtain that $D(\lambda)=0$ only when $\lambda=\lambda_0^{(2)}=1$ (where the mode is born). For the symmetric mode {++} one verifies that similar to the previous case $D(\lambda)=0$ at the point of linear limit $\lambda=\lambda_0^{(1)}=-1$, but also at $\lambda=\lambda_*=-2$, where the mode {++} bifurcates with mode {+0}. The mode {+0} (for which $Q_{1,2}^2=-\lambda/2\pm\sqrt{\lambda^2/4-1}$) exists only when $\lambda\le\lambda_*$, and at the point λ_* it has the same field distribution as mode {++} (so, we have a pitchfork-type bifurcation).

D. Surface modes in one-dimensional finite lattice

Turning now to the analysis of surface modes, by analogy with an infinite array [19], one can distinguish *fundamental* modes, having in-phase distribution of the field near the edges, and *twisted* surface modes, having out-of-phase fields in the two waveguides bordering an edge. As an example, in Fig. 2 we show the mode patterns for arrays of $M=6$ and $M=7$ waveguides. All the modes shown require a threshold power to be excited. Two different symmetric and antisymmetric fundamental surface modes bifurcate with each other at $\lambda_*^{(Ms)}$ and $\lambda_*^{(Ma)}$ (the codes of such modes are indicated in the respective panels of Fig. 2). The pairs of symmetric modes, (A,B) and (E,F), bifurcate in $\lambda_*^{(7s)}\approx-3.005$ and

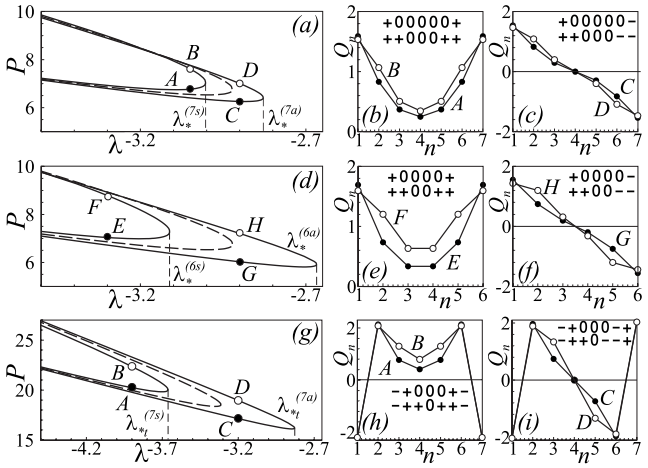

FIG. 2. P vs λ for fundamental (a), (d), and twisted (g) modes. In panels (b), (c), (e), and (f) examples of the symmetric (A,B,E,F) and antisymmetric (C,D,G,H) fundamental surface modes, as well as their classifications, are shown for $M=7$ [panels (b), (c)] and $M=6$ [panels (e), (f)]. In panels (h) and (i) symmetric (A,B) and antisymmetric (C,D) twisted surface modes for $M=7$ are shown. In all examples $\sigma=1$. For comparison, in panels (a), (d), and (g) the dashed lines represent doubled powers of the same modes in a semi-infinite waveguide array.

$\lambda_*^{(6s)}\approx-3.115$, while the bifurcation points of antisymmetric modes, (C,D) and (G,H), are given by $\lambda_*^{(7a)}\approx-2.83$ and $\lambda_*^{(6a)}\approx-2.67$. We observe that $\lambda_*^{(Ms)}<\lambda_*^{(Ma)}$ and thus the antisymmetric modes are excited at lower field intensities. Comparing the bifurcation points of the modes with different M we also observe that for large enough arrays, i.e., at $M\to\infty$, the modes are transformed in the conventional surface modes of a semi-infinite array. In this limit distinction between symmetric and antisymmetric modes disappears. Thus the presence of two boundaries of a finite array essentially modifies a surface mode. The physical reason for this is that in a vicinity of the bifurcation point the modes are weakly localized near the array edges, and the field in waveguides near the center of the array is non-negligible (see Fig. 2). This leads to interaction between the modes, supported by the two edges, which in its turn modifies the patterns. At large values of $|\lambda|$ the modes are strongly localized near the edges and interaction between them is weak, which results in the identical asymptotic behavior of symmetric and antisymmetric modes in the AC limit clearly seen in Figs. 2(a) and 2(d).

The code of the twisted mode includes more nonzero symbols in comparison with the code of the fundamental mode. So, since the symbol "0" in the code of a certain mode signifies zero field amplitude in the correspondent waveguide in the AC limit, the power of a twisted mode in the AC limit should be higher than the power of the fundamental mode. Nevertheless, as shown in Fig. 2(g), even in the vicinity of the bifurcation point twisted modes are excited at higher intensities than the fundamental modes. Also due to higher field in the center of the waveguide array (in comparison with the fundamental mode case) the interaction between two edges of the array is stronger, which is expressed by the

relation $\lambda_{*t}^{(7a)}-\lambda_{*t}^{(7s)}>\lambda_{*}^{(7a)}-\lambda_{*}^{(7s)}$ (the bifurcation points are $\lambda_{*t}^{(7s)}\approx -3.665$ and $\lambda_{*t}^{(7a)}\approx -2.83$). The main peculiarity of the diagram of the twisted modes is that surface modes A and C bifurcate with the bulk modes B and D.

To study linear stability of the modes, we follow the standard steps analyzing the eigenvalue problem linearized about the mode, where β is the spectral parameter such that $\mathrm{Im}(\beta)<0$ corresponds to a linearly unstable mode. The imaginary parts of β for the fundamental modes B, D, F, and H decrease with $\lambda\to-\infty$, i.e., the modes are unconditionally unstable (similar behavior was reported in [20]). Symmetric fundamental modes A and E are unstable, but $\mathrm{Im}(\beta)$ increase with the decreasing of λ. The antisymmetric fundamental modes C and G are unstable in the vicinity of the bifurcation point, but are stabilized at $\lambda<-3.13$ (for $M=7$) and $\lambda<-3.22$ (for $M=6$). Stability analysis of the twisted modes shows that symmetric modes A, B, and the antisymmetric mode D are unconditionally linearly unstable, while the antisymmetric mode C is stable at $\lambda<-3.87$ (these results corroborate with the results of [21] for the discrete modes of infinite array).

III. SURFACE BREATHERS

Now we consider another type of localized mode—surface breathers. Antisymmetric surface breathers can be constructed analytically for an array of $M=5$ sites. In this case, Eq. (1) possesses a solution of the following type (found using the known dynamics of a dimer [22]),

$$z(\zeta)=\frac{4C}{P}\cdot\begin{cases}\mathrm{cn}(C(\zeta-\zeta_0)/k,k), & 0<k<1,\\ \mathrm{dn}(C(\zeta-\zeta_0),1/k), & k>1,\end{cases}\tag{12}$$

where cn and dn are Jacobi elliptic functions, $z=2(|q_1|^2-|q_2|^2)/P$ is the intensity contrast, $k=C/[\sqrt{2}\varrho(P)]$ is the elliptic modulus,

$$\zeta_0=kF(\arccos[z(0)P/(4C)],k)/C.$$

$F(\phi,k)$ is the incomplete elliptic integral of the first kind,

$$C^2=\varrho^2-H/2-P^2/16-2,$$

and $\varrho=(P^2/2+2H+4)^{1/4}$. When $k\gg1$, the function

$$z(\zeta)\approx(4C/P)\{1-\sin^2[C(\zeta-\zeta_0)]/2k^2\}$$

describes a mode concentrated near the edges $n=1,5$ (see Fig. 3) and oscillating with the period $2K(1/k)/C$ ($K(k)$ is the complete elliptic integral of the first kind). In the limit $k\to\infty$ (taken at a constant power P) the Hamiltonian achieves it minimal value $H=-P^2/4-2$ and the intensity contrast becomes a constant. In that case the surface breather transforms into a fundamental surface mode (e.g., the breathers in Figs. 3(a) and 3(b) transform into the surface modes with $P=7$, $\lambda=-3.5$, $H=-14.25$ and $P=12$, $\lambda=-6$, $H=-38$, respectively). Thus a surface breather can be excited from the fundamental surface mode by small detuning of its Hamiltonian from the minimum. We used this idea to construct the antisymmetric surface breathers for arrays of $M=7$ and $M=8$ waveguides [Figs. 3(c) and 3(d)], which cannot be constructed analytically. Notice that when the Hamiltonian possesses its minimal value, the surface breathers of Figs. 3(c) and 3(d) transform into stationary modes with $M=7$, $\lambda=-6$, $H=-38.185$ and $M=8$, $\lambda=-6$, $H=-38.192$, respectively.

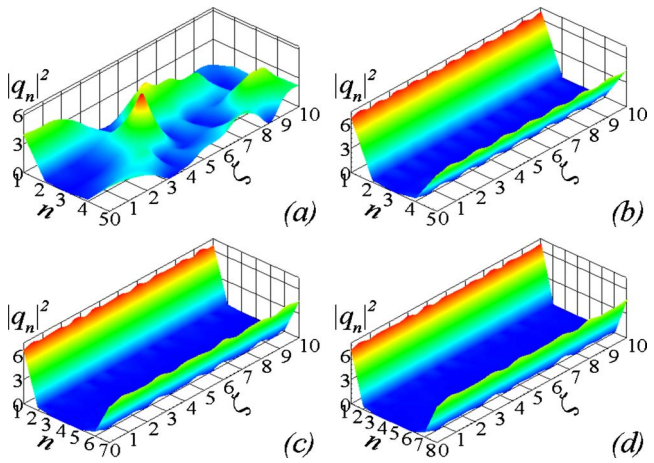

FIG. 3. (Color online) Surface breather for (a) $M=5$, $P=7$, $H=-14.175$; (b) $M=5$, $P=12$, $H=-37.602$; (c) $M=7$, $P=12.021$, $H=-37.463$; and (d) $M=8$, $P=12.022$, $H=-37.471$, excited by noise.

We tested the stability of breathers by direct numerical solution of differential Eq. (1), perturbing the initial profiles by noise with an amplitude of order of 10% of Q_n in each waveguide. The breather, depicted in Fig. 3(a), has shown unstable behavior, while breathers of Figs. 3(b)–3(d) demonstrated a stable one. Like in the case of the surface modes, increasing of $|\lambda|$ results in stabilization of a surface mode.

The case $M=4$ also allows for analytical construction of symmetric ($b=1$) and antisymmetric ($b=-1$) breathers. Now $z=z_1+6f'(z_1)/[24\wp(P(\zeta-\zeta_0)/4;g_2,g_3)-f''(z_1)]$, where z_1 is a root of the polynomial $f(z)=a_4+a_3z+a_2z^2+a_1z^3-z^4$, $a_4=16(4-4H^2/P^2-H-P^2/16)/P^2$, $a_3=64b(H+P^2/8)/P^3$, $a_2=-8(10+2H+P^2/4)/P^2$, $a_1=8b/P$, and $\wp(x;g_2,g_3)$ is the Weierstrass elliptic function with $g_2=a_2^2/12-a_1a_3/4-a_4$ and $g_3=a_1a_2a_3/48+a_3^2-a_2^3/216-(a_1^2/16+a_2/6)a_4$. The character of oscillations of the field along the waveguides is determined by $\Delta=g_2^3-27g_3^2$: for $\Delta\neq0$ the solutions are oscillatory about a nonzero average, but for $\Delta=0$ the solutions are aperiodic.

IV. CORNER AND EDGE MODES

Now we discuss surface modes of a 2D finite $M\times M$ array, where each waveguide is coupled with the nearest neighbors. The system is described by a coupled 2D DNLS equation,

$$i\dot{q}_{n,m}+\sum_{m'=1}^{M}(\delta_{m',m+1}+\delta_{m',m-1})q_{n,m'}+\sum_{n'=1}^{M}(\delta_{n',n+1}+\delta_{n',n-1})q_{n',m}+\sigma|q_{n,m}|^2q_{n,m}=0.\tag{13}$$

Now the total power is given by $P=\Sigma_{n,m=1}^{M}|q_{n,m}|^2$ and the

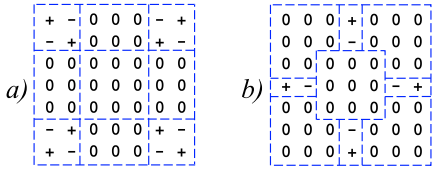

FIG. 4. (Color online) Examples of the fully symmetric corner (a) and edge (b) modes. The dashed lines outline empty and simple blocks.

symmetry reductions of the stationary modes $q_{n,m}(\zeta) = Q_{n,m}\exp(-i\lambda\zeta)$ are as follows: if the $Q_{n,m}$ is a solution of Eq. (13) for a definite λ and $\sigma=+1$, then $(-1)^{n+m}Q_{n,m}$ is a solution for $-\lambda$ and $\sigma=-1$.

Similar to the 1D case, each mode can be coded on a 2D *map* by an array of $M\times M$ symbols −, 0, and + (see examples in Fig. 4), corresponding to its AC limit ($P\to\infty$). Splitting the array into blocks, we call "empty" a block consisting of all zeros and "simple" a simply connected block having no zeros. Now we define a *corner* mode as a mode on a square array consisting of only simple blocks at the corners, separated by empty blocks of higher dimensions [see an example in Fig. 4(a)]. Being interested only in modes of a definite symmetry we impose additional constraints: $q_{n,m} = q_{M+1-n,m} = q_{n,M+1-m}$ (for fully symmetric modes), $q_{n,m} = -q_{M+1-n,m} = q_{n,M+1-m}$ (for symmetric-antisymmetric modes), and $q_{n,m} = -q_{M+1-n,m} = -q_{n,M+1-m}$ (for fully antisymmetric modes). Similarly we identify an *edge* mode, whose code consists of simple blocks bordering edges of the array, but separated from each other and from the corners by empty blocks [see the example in Fig. 4(b)]. Symmetry constrains for the edge mode are as follows: $q_{n,m} = q_{m,n} = q_{M+1-m,M+1-n}$ (for fully symmetric modes), $q_{n,m} = q_{m,n} = -q_{M+1-m,M+1-n}$ (for symmetric-antisymmetric modes), and $q_{n,m} = -q_{m,n} = -q_{M+1-m,M+1-n}$ (for fully antisymmetric modes).

We restrict the consideration to the lowest-power fundamental modes, i.e., modes coded by one-site simple blocks. We found that similar to the 1D case both corner and edge fully antisymmetric modes (C and F in Fig. 5, correspondingly) require lower threshold power of excitations than other types of modes, while the fully symmetric modes (A and D in Fig. 5, correspondingly) are excited at higher powers (see upper panel in Fig. 5). At the same time the distinction between the properties of the fully symmetric, symmetric-antisymmetric, and fully antisymmetric edge modes is stronger than the distinction between the properties of similar types of corner modes. This occurs due to the smaller distance (and hence stronger interaction) between the excitation centered at four edges in comparison with excitations centered at four corners (compare, e.g., field patterns for modes A and D, B and E, C and F in Fig. 5). The stability analysis shows that fully symmetric and symmetric-antisymmetric modes A, B, D, E are unstable, but their instability increments $\mathrm{Im}(\beta)<0$ increase as λ decreases. The fully antisymmetric modes C and F are stabilized at $\lambda<-4.74$ and $\lambda<-5.4$, respectively.

V. CONCLUSION

We have reported the complete families of (edge and corner) surface modes in arrays of 1D and 2D waveguides, presenting the classification exhausting all possible stationary excitations. It has been shown that the surface modes belong to one-parametric branches of solutions, which bifurcate either with other surface or with bulk modes, when the total power is properly changed. We have also found two-periodic modes, surface breathers, whose intensity periodically oscillates staying localized about the edge of the array, and described a way of excitations of breathers starting with the respective surface modes. The reported solutions, being well localized at the two (or four in the 2D case) surfaces and at the same time showing nonzero intensity in the bulk of the array, can be of significant practical importance, by analogy with the polaritons assisting extraordinary transmittancy [11]. Meantime we emphasize a number of open questions which were left unanswered by the present research. Among those we mention thorough study of the linear stability of the surface breathers, mathematical justification of the complete classification of the two-dimensional modes starting with the AC limit. These issues as well as specific practical outputs will be addressed elsewhere.

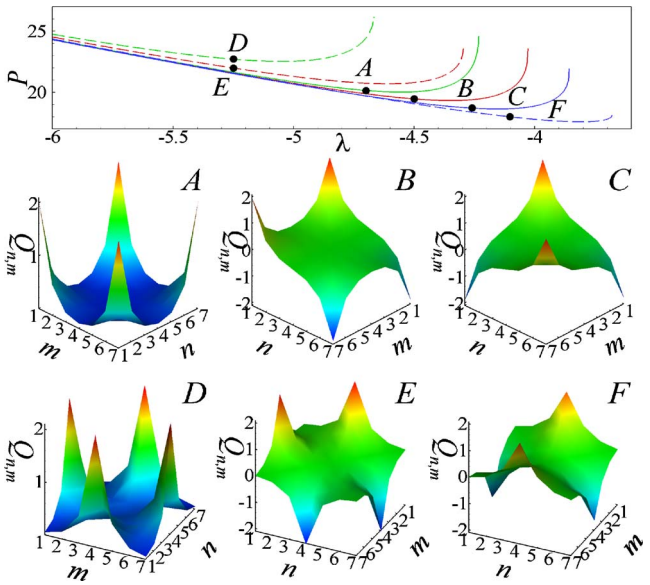

FIG. 5. (Color online) The total intensity P vs the propagation constant λ (upper panel) for corner (solid lines) and edge (dashed lines) modes. Examples of the patterns of the corner [panels (A)–(C)] and edge [panels (D)–(F)] modes are shown for $M=7$ and $\sigma=1$. (A) and (D) are fully symmetric modes, (B) and (E) are symmetric-antisymmetric modes, and (C) and (F) are fully antisymmetric modes.

ACKNOWLEDGMENTS

Y.V.B. was supported by FCT Grant No. SFRH/PD/20292/2004. V.V.K. acknowledges support of the Secretaria de Stado de Universidades e Investigación (Spain) under Grant No. SAB2005-0195. The work was supported by the FCT and European program FEDER (Grant No. POCI/FIS/56237/2004).

[1] I. E. Tamm, Z. Phys. **76**, 849 (1932).
[2] P. Berini, R. Charbonneau, N. Lahoud, and G. Mattiussi, J. Appl. Phys. **98**, 043109 (2005).
[3] See, e.g., A. G. Brolo, R. Gordon, B. Leathem, and K. L. Kavanagh, Langmuir **20**, 4813 (2004).
[4] K. G. Makris, S. Suntsov, D. N. Christodoulides, G. I. Stegeman, and A. Hache, Opt. Lett. **30**, 2466 (2005).
[5] S. Suntsov, K. G. Makris, D. N. Christodoulides, G. I. Stegeman, A. Hache, R. Morandotti, H. Yang, G. Salamo, and M. Sorel, Phys. Rev. Lett. **96**, 063901 (2006).
[6] M. I. Molina, R. A. Vicencio, and Y. S. Kivshar, Opt. Lett. **31**, 1693 (2006).
[7] Y. V. Kartashov, L. Torner, and V. A. Vysloukh, Phys. Rev. Lett. **96**, 073901 (2006).
[8] K. G. Makris, J. Hudock, D. N. Christodoulides, G. I. Stegeman, O. Manela, and M. Segev, Opt. Lett. **31**, 2774 (2006); H. Susanto, P. G. Kevrekidis, B. A. Malomed, R. Carretero-Gonzalez, and D. J. Franzeskakis, Phys. Rev. E **75**, 056605 (2007).
[9] R. A. Vicencio, S. Flach, M. I. Molina, and Y. S. Kivshar, Phys. Lett. A **364**, 274 (2007).
[10] R. E. Camley and D. L. Mills, Phys. Rev. B **29**, 1695 (1984).
[11] T. W. Ebbesen, H. J. Lezec, H. F. Ghaemi, T. Thio, and P. A. Wolff, Nature (London) **391**, 667 (1998).
[12] G. L. Alfimov, V. A. Brazhnyi, and V. V. Konotop, Physica D **194**, 127 (2004).
[13] D. N. Christodoulides and R. I. Joseph, Opt. Lett. **13**, 794 (1988).
[14] A. Scott, *Nonlinear Science: Emergence of Coherent Structures* (Oxford University Press, New York, 1999).
[15] V. A. Brazhnyi and V. V. Konotop, Mod. Phys. Lett. B **18**, 627 (2004).
[16] See, e.g., D. Hennig and G. Tsironis, Phys. Rep. **307**, 333 (1999); P. G. Kevrekidis, K. Ø. Rasmussen, and A. R. Bishop, Int. J. Mod. Phys. B **15**, 2833 (2001).
[17] R. S. MacKay and S. Aubry, Nonlinearity **7**, 1623 (1994).
[18] R. Bellman, *Introduction to Matrix Analysis* (McGraw-Hill Education, New York, 1970).
[19] S. Darmanyan, A. Kobyakov, and F. Lederer, Zh. Eksp. Teor. Fiz. **113**, 1253 (1998) [JETP **86**, 682 (1998)].
[20] Y. V. Kartashov, V. A. Vysloukh, D. Mihalache, and L. Torner, Opt. Lett. **31**, 2329 (2006).
[21] D. E. Pelinovsky, P. G. Kevrekidis, and D. J. Frantzeskakis, Physica D **212**, 1 (2005).
[22] V. M. Kenkre and D. K. Campbell, Phys. Rev. B **34**, 4959 (1986); S. Raghavan, A. Smerzi, S. Fantoni, and S. R. Shenoy, Phys. Rev. A **59**, 620 (1999).